

23 assessed its pathogenicity in hACE2 mice. We found that the GX_P2V(short_3UTR)
24 clone can infect hACE2 mice, with high viral loads detected in both lung and brain
25 tissues. This infection resulted in 100% mortality in the hACE2 mice. We surmise that
26 the cause of death may be linked to the occurrence of late brain infection.

27 The GX_P2V(short_3UTR) mutant, initially isolated from the early passages of
28 the GX_P2V sample (6), and the GX_P2V virus itself, have not been studied in terms
29 of their adaptive mutations in cell cultures. To obtain a genetically homogenous clone
30 for animal experiments, we cloned the passaged mutant through two successive plaque
31 assays. Eight viral clones were chosen for next-generation sequencing (National
32 Genomics Data Center of China, GSA: CRA014225). These clones, when compared
33 with the genome of the original mutant (6), all shared four identical mutations:
34 ORF1ab_D6889G, S_T730I, S_K807N, and E_A22D (Supporting Information, Table
35 S1). Clone 7, named as GX_P2V C7, was randomly selected for the evaluation of viral
36 pathogenicity in hACE2 mice (Figure 1A). The hACE2 mouse model expressing
37 human ACE2 under control of the CAG promoter was developed using random
38 integration technology by Beijing SpePharm Biotechnology Company.

39 We initially assessed whether GX_P2V C7 could cause disease in hACE2 mice by
40 monitoring daily weight and clinical symptoms. A total of four 6 to 8-week-old hACE2
41 mice were intranasally infected with a dosage of 5×10^5 plaque-forming units (pfu) of
42 the virus. Four mice inoculated with inactivated virus and four mock-infected mice
43 were used as controls. Surprisingly, all the mice that were infected with the live virus
44 succumbed to the infection within 7-8 days post-inoculation, rendering a mortality rate

45 of 100% (Figure 1B). The mice began to exhibit a decrease in body weight starting from
46 day 5 post-infection, reaching a 10% decrease from the initial weight by day 6 (Figure
47 1C). By the seventh day following infection, the mice displayed symptoms such as
48 piloerection, hunched posture, and sluggish movements, and their eyes turned white.
49 The criteria for clinical scoring of the mice and the daily clinical scores post-infection
50 with GX_P2V C7 are provided in the Supporting Information, Figure S1.

51 We then evaluated the tissue tropism of GX_P2V C7 in hACE2 mice. Using the
52 infection method described above, eight hACE2 mice were infected, eight mice were
53 inoculated with inactivated virus, and another eight mock-infected mice were used as
54 controls. The organs of four randomly selected mice in each group were dissected on
55 days 3 and 6 post-infection for quantitative analysis of viral RNA and titer. We detected
56 significant amounts of viral RNA in the brain, lung, turbinate, eye, and trachea of the
57 GX_P2V C7 infected mice (Figure 1D), whereas no or a low amount of viral RNA was
58 detected in other organs such as the heart, liver, spleen, kidneys, tongue, stomach, and
59 intestines. Specifically, in lung samples, we detected high viral RNA loads on days 3
60 and 6 post-infection, with no significant difference between these two time points (~
61 6.3 versus ~ 5.8 Log₁₀[copies/mg]). In brain samples, on day 3 post-infection, viral
62 RNA was detected in all four infected mice, with an average value of 5.4
63 Log₁₀[copies/mg]. Notably, by day 6 post-infection, we detected exceptionally high
64 viral RNA loads (~ 8.5 Log₁₀[copies/mg]) in the brain samples from all four infected
65 mice (Figure 1D). On days 3 and 6 post-infection, the viral RNA loads in the turbinate
66 were similar, approximately 4.1 and 3.9 Log₁₀[copies/mg], respectively. The viral RNA

67 loads in the trachea and eyes of the mice surpassed the limit of detection only on day 6
68 post-infection, with values of 2.6 and 3.8 Log₁₀[copies/mg], respectively. Regarding the
69 infectious viral titers, lung tissues at day 3 post-infection had a value of ~ 1.8
70 Log₁₀[pfu/mg], which decreased to ~ 0.5 Log₁₀[pfu/mg] by day 6. Importantly, the
71 highest infectious titers were detected in the brain on day 6, which was significantly
72 greater than that on day 3 (~ 0.9 vs ~ 4.8 Log₁₀[pfu/mg]) (Figure 1E). Additionally,
73 there were no significant differences in the infectious titers in the turbinate between day
74 3 (~ 0.9 Log₁₀[pfu/mg]) and day 6 (~ 1.2 Log₁₀[pfu/mg]) (Figure 1E). By day 6,
75 approximately 2.0 Log₁₀[pfu/mg] was detected in the eyes of two mice. Neither
76 inactivated GX_P2V C7 nor mock infection caused death or any clinical symptoms in
77 the mice (Figure 1B-C and Supporting Information, Figure S2). In summary, in the mice
78 infected with live virus, the viral load in the lungs significantly decreased by day 6;
79 both the viral RNA loads and viral titers in the brain samples were relatively low on
80 day 3, but substantially increased by day 6. This finding suggested that severe brain
81 infection during the later stages of infection may be the key cause of death in these mice.

82 To determine the mechanisms underlying GX_P2V C7-induced death in hACE2
83 mice, we examined the pathological changes, presence of viral antigens, and cytokine
84 profiles in the lung and brain tissues of the mice on days 3 and 6 post-infection (Figure
85 1F-G, and Supporting Information, Figure S3 and S4). On both days, compared to those
86 of control mice, the lungs of infected mice showed no significant pathological
87 alterations, with only minor inflammatory responses due to slight granulocyte
88 infiltration (Figure 1F). On day 3 post-infection, shrunken neurons were visible in the

89 cerebral cortex of the mice. By day 6, in addition to the shrunken neurons, there was
90 focal lymphocytic infiltration around the blood vessels, although no conspicuous
91 inflammatory reaction was observed (Figure 1G). Upon staining for viral nucleocapsid
92 protein via immunohistochemistry, viral antigens were detected in both the lungs and
93 brains on days 3 and 6 post-infection, with extensive viral antigens notably present in
94 the brain on day 6 (Figure 1F-G). These findings align with the viral RNA load
95 assessments in the lung and brain tissues (Figure 1D). We also performed a Luminex
96 cytokine assay to detect 31 cytokines/chemokines in the lung and brain tissues of the
97 mice (Supporting Information, Figure S3 and S4). Consistent with the pathological
98 findings, there were slight increases or decreases in the levels of many
99 cytokines/chemokines in lung and brain tissues compared to those in control tissues,
100 but the levels of key inflammatory factors, such as IFN- γ , IL-6, IL-1 β , and TNF- α , did
101 not significantly change. In brief, these analyses revealed that GX_P2V C7 infection in
102 hACE2 mice did not lead to severe inflammatory reactions, a finding that aligns with
103 previous reports by Zhengli Shi's group using GX_P2V infection in two different
104 hACE2 mouse models (5), as well as our own findings in the golden hamster model (6).

105 To the best of our knowledge, this is the first report showing that a SARS-CoV-2-
106 related pangolin coronavirus can cause 100% mortality in hACE2 mice, suggesting a
107 risk for GX_P2V to spill over into humans. Our findings are evidently inconsistent with
108 those of Zhengli Shi *et al.* (5), who tested the virulence of GX_P2V in two different
109 hACE2 mouse models. It is important to note that we did not isolate the wild-type
110 GX_P2V strain. The study by Zhengli Shi *et al* tested the GX_P2V(short_3UTR)

111 variant that we reported. However, the adaptative evolutionary changes of this variant
112 during their laboratory culture remain understudied. In fact, according to additional
113 infection experiments, the uncloned GX_P2V(short_3UTR) also resulted in 100%
114 mortality in hACE2 mice. Due to the propensity of coronaviruses to undergo adaptive
115 mutation during passage culture, we cloned and analyzed mutations in
116 GX_P2V(short_3UTR), focusing specifically on the pathogenicity of the cloned strains.
117 The high pathogenicity mechanism of GX_P2V C7 in hACE2 mice, in the absence of
118 the wild-type GX_P2V control, requires further investigation. Compared to the original
119 sequence of GX_P2V(short_3UTR), GX_P2V C7 has two amino acid mutations in the
120 spike protein. Given the close relationship between coronavirus virulence and spike
121 protein mutations (7), it is possible that GX_P2V C7 has undergone a virulence-
122 enhancing mutation. However, it is important to note that our hACE2 mouse model
123 may be relatively unique. The company has not yet published a paper on this hACE2
124 mouse model, but our results suggest that hACE2 may be highly expressed in the mouse
125 brain. Additionally, according to the data provided by the company, these hACE2 mice
126 have abnormal physiology, as indicated by relatively reduced serum triglyceride,
127 cholesterol, and lipase levels, compared to those of wild-type C57BL/6J mice. In
128 summary, our study provides a unique perspective on the pathogenicity of GX_P2V
129 and offers a distinct alternative model for understanding the pathogenic mechanisms of
130 SARS-CoV-2-related coronaviruses.

131

132 Lai Wei^{1,#}, Shuiqing Liu^{1,#}, Shanshan Lu^{1,#}, Shengdong Luo², Xiaoping An¹, Huahao

133 Fan¹, Weiwei Chen², Erguang Li^{3,*}, Yigang Tong^{1,*}, Lihua Song^{1,*}

134 ¹ Beijing Advanced Innovation Center for Soft Matter Science and Engineering,

135 College of Life Science and Technology, Beijing University of Chemical Technology,

136 Beijing, China. ²Research Center for Clinical Medicine, The Fifth Medical Center of

137 PLA General Hospital, Beijing, China. ³State Key Laboratory of Pharmaceutical

138 Biotechnology, Medical School, Nanjing University, China

139 #Contributed equally.

140 *email: erguang@nju.edu.cn; tong.yigang@gmail.com; songlihua@gmail.com

141

142 REFERENCES

143 1. Liu P, Chen W, Chen JP. Viral Metagenomics Revealed Sendai Virus and

144 Coronavirus Infection of Malayan Pangolins (*Manis javanica*). *Viruses*. 2019 Oct

145 24;11(11).

146 2. Lam TT, Jia N, Zhang YW, Shum MH, Jiang JF, Zhu HC, et al. Identifying SARS-

147 CoV-2-related coronaviruses in Malayan pangolins. *Nature*. 2020 Jul;583(7815):282-5.

148 3. Xiao K, Zhai J, Feng Y, Zhou N, Zhang X, Zou JJ, et al. Isolation of SARS-CoV-

149 2-related coronavirus from Malayan pangolins. *Nature*. 2020 Jul;583(7815):286-9.

150 4. Huang XY, Chen Q, Sun MX, Zhou HY, Ye Q, Chen W, et al. A pangolin-origin

151 SARS-CoV-2-related coronavirus: infectivity, pathogenicity, and cross-protection by

152 preexisting immunity. *Cell Discov*. 2023 Jun 17;9(1):59.

153 5. Liu MQ, Lin HF, Li J, Chen Y, Luo Y, Zhang W, et al. A SARS-CoV-2-Related

154 Virus from Malayan Pangolin Causes Lung Infection without Severe Disease in Human

155 ACE2-Transgenic Mice. *J Virol*. 2023 Feb 28;97(2):e0171922.

156 6. Lu S, Luo S, Liu C, Li M, An X, Li M, et al. Induction of significant neutralizing
157 antibodies against SARS-CoV-2 by a highly attenuated pangolin coronavirus variant
158 with a 104nt deletion at the 3'-UTR. *Emerg Microbes Infect.* 2023 Dec;12(1):2151383.

159 7. Roberts A, Lamirande EW, Vogel L, Jackson JP, Paddock CD, Guarner J, et al.
160 Animal models and vaccines for SARS-CoV infection. *Virus Res.* 2008 Apr;133(1):20-
161 32.

162

163 **ACKNOWLEDGEMENTS**

164 This work was supported by NSFC-MFST project (China–Mongolia) (grant number
165 32161143027), National Key R&D Program of China (2021YFC2301804) and
166 Biosafety Special Program (No. 19SWAQ 13).

167 **ETHICS STATEMENT**

168 All animals involved in this study were housed and cared for in an AAALAC
169 (Association for Assessment and Accreditation of Laboratory Animal Care) accredited
170 facilities. The procedure for animal experiments (IACUC-2019-0027) was approved by
171 the Institutional Animal Care and Use Committee of the Fifth Medical Center, General
172 Hospital of the Chinese People's Liberation Army, and complied with IACUC standards.

173 **AUTHOR CONTRIBUTIONS**

174 L.Song conceived and designed the study and wrote the manuscript. L.W., S.Liu, S.Lu.,
175 and S.Luo. performed the experiments and analyzed the data. X.A., H.F., W.C., E.L.
176 and Y.T. analyzed the data and edited the manuscript. L.W. and L.Song wrote the
177 manuscript and all the authors approved the manuscript.

178 **CONFLICT OF INTERESTS**

179 The authors declare no competing interests.

180 **SUPPORTING INFORMATION**

181 Additional Supporting Information for this article can be found online at

182 **DATA AVAILABILITY**

183 All the data supporting the findings of this study are available within the article and
184 the Supporting Information, or from the corresponding author upon reasonable
185 request.

186 **ORCID**

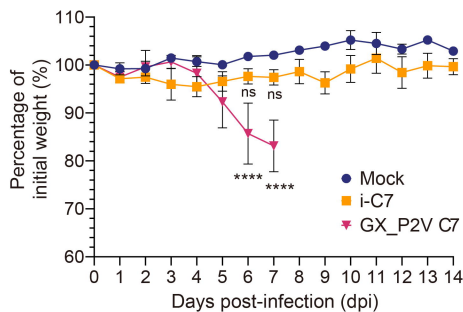
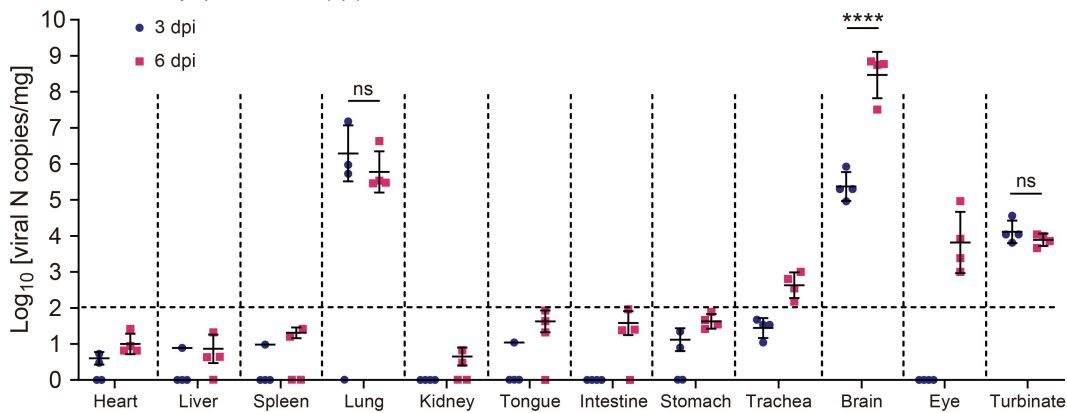
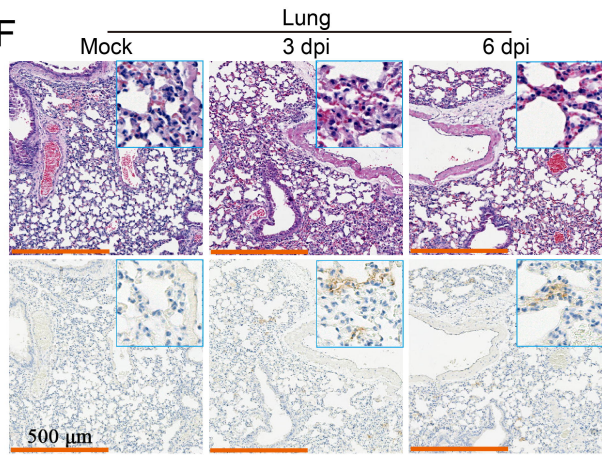
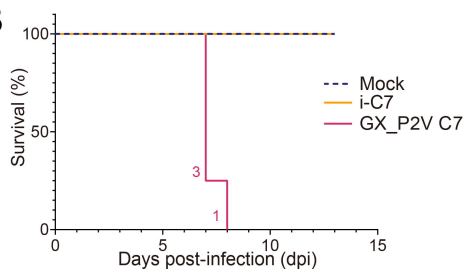
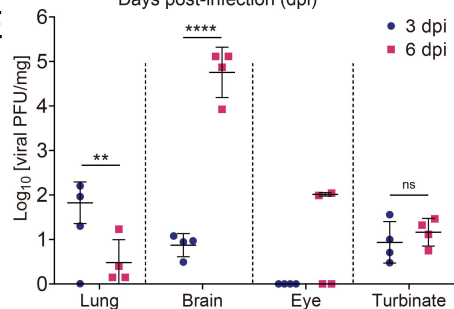
187 Lihua Song, <https://orcid.org/0000-0002-7299-5719>

188 **Figure 1: Characterization of a lethal infection model in human ACE2-transgenic**
189 **mice caused by the attenuated SARS-CoV-2-related pangolin coronavirus**
190 **GX_P2V C7. A** Mutations in GX_P2V C7 compared to the GX_P2V(short_3UTR)
191 isolate (NCBI accession number: MW532698). The four identical mutations are shown
192 in bold. **B** Survival of hACE2 transgenic mice following intranasal infection with
193 GX_P2V C7 ($n = 4$), inactivated GX_P2V C7 (i-C7, $n = 4$), and mock infection ($n = 4$).
194 The number of deceased mice on each specific day is annotated on the left of the
195 survival curve. **C** Percentage of initial weight of hACE2 transgenic mice after intranasal
196 infection with GX_P2V C7 ($n = 4$), i-C7 ($n = 4$), and mock infection ($n = 4$). The
197 statistical significance of the differences between mock-infected ($n = 4$, blue dots) and
198 GX_P2V C7-infected ($n = 4$, red dots) or i-C7-infected mice ($n = 4$, orange dots) at 6
199 or 7 dpi are shown. The error bars represent the means \pm SDs. **D** Quantification of
200 GX_P2V N gene copies in heart, liver, spleen, lung, kidney, tongue, intestine, stomach,
201 trachea, brain, eye, and turbinate homogenates at 3- and 6-day post-infection (dpi) ($n =$
202 4 per group). The limit of detection (LOD) for viral RNA loads in the original samples
203 was $\text{Log}_{10}[10^2 \text{ copies/mg}]$. The error bars represent the means of $\text{Log}_{10}[\text{copies/mg}] \pm$
204 SDs. The significances of the comparisons in the lung, brain, and turbinate are shown.
205 **E** Infectious viral titers in lung, brain, eye, and turbinate homogenates were measured
206 by plaque forming assay at 3 and 6 dpi ($n = 4$ per group). The statistical significance of
207 the differences in the lung, brain, and turbinate are shown. The error bars represent
208 means of $\text{Log}_{10}[\text{pfu/mL}] \pm$ SDs. **F, G** Hematoxylin and eosin (H&E) staining and
209 immunohistochemical (IHC) staining with an anti-SARS-CoV-2 N-specific antibody

210 (SARS-CoV-2) revealed viral antigen–positive cells (brown) in the lung (**F**) and brain
211 (**G**), as shown at high magnification in the inset. Scale bars, 500 μm (**F**) and 1 mm (**G**),
212 respectively. $*P < 0.05$, $**P < 0.01$, $***P < 0.001$, $****P < 0.0001$, $P > 0.05$, not
213 significant (ns); two-way ANOVA followed by Sidak’s multiple comparison test.

A

Mutation	Codon change	Substitution	CDS Location
1807 A to G	GGA to GGG		ORF1ab
6501 C to U	ACA to AUA	T to I	ORF1ab
19694 C to U	ACA to AUA	T to I	ORF1ab
20930 A to G	GAU to GGU	D to G	ORF1ab
23727 C to U	ACU to AUU	T to I	S
23959 A to C	AAA to AAC	K to N	S
26274 C to A	GCU to GAU	A to D	E
29227 C to U	UAC to UAU		N

C**D****F****B****E****G**